JOURNAL OF SPACECRAFT AND ROCKETS
Vol. 36, No. 2, March–April 1999

Engineering Aerothermal Analysis for X-34 Thermal Protection System Design

Kathryn E. Wurster,* Christopher J. Riley,† and E. Vincent Zoby‡
NASA Langley Research Center, Hampton, Virginia 23681

Design of the thermal protection system for any hypersonic flight vehicle requires determination of both the peak temperatures over the surface and the heating-rate history along the flight profile. The process used to generate the time-dependent aerothermal environments for design of the X-34 thermal protection system is described. The process evolved from a relatively simplistic approach based solely on engineering methods applied to critical areas to an integrated approach using ground-test data with detailed computational and engineering methods to predict the aeroheating over the entire vehicle. A brief description of the trajectory development leading to the selection of the thermal protection system design trajectory is included. Comparisons of engineering heating predictions with wind-tunnel test data and with results obtained using a Navier–Stokes flowfield code and an inviscid/boundary-layer method are shown. Good agreement is demonstrated among all of these methods for both the ground-test condition and the peak heating flight condition.

Nomenclature

h = heat transfer coefficient, Btu-s/ft^4 or lbm/ft^2-s
L = reference length, in.
M = Mach number
$\dot{q}$ = heat transfer rate, Btu/ft^2-s
Re = Reynolds number
x = axial location, in.
y = spanwise location, in.
α = angle of attack, deg
δ = control surface deflection, deg
ε = emissivity

Subscripts

BF = body flap
cl = centerline (℄)
el = elevon
FR = Fay–Riddell
min = MINIVER
ref = reference value
∞ = freestream conditions

Introduction

CONTINUED human presence in space will soon require upgrade or replacement of the current Space Transportation System. Joint NASA/industry partnerships have been formed to develop and test the technology required to provide cost-effective, yet reliable access to space. The primary goal of the Reusable Launch Vehicle (RLV) Technology Program[1] is to provide affordable access to space. Development and flight of the suborbital X-34 vehicle is an integral part of the RLV program and is intended to address numerous operations, manufacturing, and other technology issues that can best be evaluated through demonstration on an actual flight vehicle. One of the key technologies to be demonstrated is that of an operationally effective thermal protection system (TPS).

Aerospace vehicles, such as the X-34, that reach hypersonic speeds generally require protection of the vehicle structure from aerodynamic heating. The TPS can be either active or passive. Active systems typically use onboard coolant pumped through pipes behind the external surface or employ heat pipes that use capillary action to redistribute the heat from hotter areas of the vehicle to cooler ones. A passive system, such as that employed on the X-34, takes advantage of the insulative properties of the TPS materials to hold a significant portion of the incident heat until it is radiated or convected away from the vehicle. The two critical parameters that determine the TPS options suitable for a given vehicle and trajectory are the peak-heating rate and the integrated heating over the time of the flight profile. The former determines the maximum temperature environment, and thus the material options, and the latter determines the thickness distribution of the insulative TPS material required to protect the surface. Except for the nosecap and wing leading edges [where silicone impregnated reusable ceramic ablator (SIRCA)[2] tile is used], the X-34 is protected with flexible-blanket or felt systems. At the request of the lead contractor, Orbital Sciences Corporation (OSC), the NASA Langley Research Center (LaRC) accepted the task to define the aerothermal environment for the surface areas protected by the flexible blanket and felt systems. The flexible blanket and felt systems are discussed in Ref. 3. Preliminary estimates of the heating to the stagnation areas will be included in this paper, but the bulk of the stagnation area analysis, both environment prediction and SIRCA tile design, has been performed at the NASA Ames Research Center (ARC) and is described in Refs. 2 and 4.

In the past, engineering methods have been used almost exclusively to predict external thermal environments and define TPS requirements for hypersonic flight vehicles. The advent of high-speed computers that reduce the time required to produce a computational solution has enabled incorporation of detailed flowfield methods much earlier in the design process. However, limited resources and the complexity of the typical vehicle configuration generally preclude the generation of a sufficient number of computational solutions to adequately define the heating histories for TPS definition. The recent development of experimental wind-tunnel techniques,[5] whereby global heating distributions over the vehicle can be measured rapidly and at relatively low cost, also allows incorporation of experimental results at an early stage of the design process. These measured data are currently limited by the inability of the wind tunnel to reproduce the actual flight environment (flight Reynolds numbers and reacting chemistry). The primary focus of this paper is to describe how wind-tunnel and computational-fluids results have been coupled with engineering methods to predict the

Received March 3, 1998; revision received Dec. 30, 1998; accepted for publication Dec. 30, 1998.

*Senior Research Engineer, Vehicle Analysis Branch, Space Systems and Concepts Division. Senior Member AIAA.
†Research Engineer, Aerothermodynamics Branch, Aero- and Gas-Dynamics Division. Senior Member AIAA.
‡Senior Research Engineer, Aerothermodynamics Branch, Aero- and Gas-Dynamics Division. Fellow AIAA.

Fig. 1 Artist's concept of the X-34 configuration in flight.

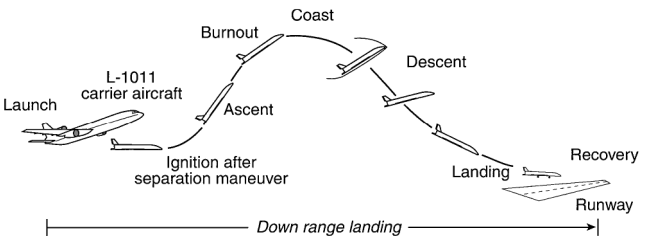

Fig. 2 Typical X-34 flight profile.

time-dependent thermal environments required for the design of the X-34 TPS. The validity of the process is demonstrated using an intermediate check case.

Vehicle/Mission Description

The X-34 Testbed Technology Demonstrator represents a key element of the RLV program. Originally envisioned as an operational vehicle with the capability to deliver relatively small payloads (1000–2000 lb) to low Earth orbit, the program was restructured in early 1996 to focus on the demonstration of RLV technologies[6] such as reusable cryogenic fuel tanks and insulation, composite primary structures, and advanced TPS concepts and materials. OSC, formerly teamed with Rockwell International in the initial effort,[7] was selected in June of 1996 to lead the redirected program. An artist's concept of the X-34 flight vehicle is shown in Fig. 1. Compared to the Shuttle orbiter, the vehicle is relatively small with dimensions of approximately 58 ft in length, 28 ft in wing span, and 12 ft in height (measured from the bottom of the fuselage to the tip of the vertical tail). An illustration of a typical flight profile is shown in Fig. 2. The vehicle is designed to be air-launched from an L-1011 at a Mach number of about 0.7, to ignite its 60-klb-thrust bipropellent (LOX/kerosene) engine, to accelerate to speeds up to Mach 8, to reach altitudes up to 250 kft, and finally to coast to a horizontal landing on a conventional runway.

Analysis Tools

MINIVER

MINIVER[8] is a versatile engineering code that uses various well-known approximate heating methods, together with simplified flowfields and geometric shapes to model the vehicle. Postshock and local flow properties based on normal-shock or sharp-cone entropy conditions are determined in MINIVER through user selection of the various shock shape and pressure options. The calculations can be based on perfect-gas or equilibrium-air chemistry. Angle-of-attack (AOA) effects are simulated through the use of either an equivalent tangent-cone or an approximate crossflow option.[9] The flow can be calculated for either two- or three-dimensional surfaces. However, the three-dimensional effects are available only through the use of the Mangler transformation[10] for flat-plate to sharp-cone conditions. MINIVER has been used extensively as a preliminary design tool in government and industry and has demonstrated excellent agreement with more detailed solutions for stagnation and windward acreage areas on a wide variety of vehicle configurations.[11–14] The prediction of accurate thermal environments with an engineering code is certainly based in part on the experience of the analyst. A major part of that experience is the understanding of the code limitations.

LATCH

The LATCH code[15] employs an inviscid/boundary-layer methodology that is used to compute laminar and turbulent surface heating rates on three-dimensional vehicles at AOA. An axisymmetric analog concept for three-dimensional boundary layers is used in conjunction with a generalized body-fitted coordinate system and an approximate heating method developed by Zoby.[11,16,17] The LATCH code requires far less computational resources than a full boundary-layer solution. LATCH has been shown to provide accurate results for both wind-tunnel and flight conditions[15,18–20] and is described in detail in Ref. 15.

Inviscid Solutions

For the purpose of this study, the inviscid solutions required for use with the LATCH code were computed using either the Data-Parallel Lower-Upper Relaxation (DPLUR) method[21,22] or the LAURA[23,24] run in the inviscid mode. Use of these two codes, which take advantage of different computer architectures, allowed solutions to be run concurrently on different machines, generating a greater number of solutions than would have been possible using a single computer resource. Both codes utilize rectangularly ordered structured grids as required for compatibility with LATCH. LATCH results for the peak heating condition computed using the DPLUR and the LAURA inviscid solution are shown to be in good agreement,[19] both with each other and with a detailed viscous thin-layer Navier–Stokes (N–S) solution computed using LAURA. The LAURA viscous solution is described in detail in Ref. 25. Previous heating studies on a wide variety of vehicles including the Space Shuttle orbiter,[26] the Lockheed X-33 (Ref. 20), HL-20 (Ref. 27), and Reentry-F (Ref. 28) have demonstrated the accuracy of the LAURA solutions computed for both flight and wind-tunnel conditions.

Wind-Tunnel Test Techniques

Advances in wind-tunnel test techniques have recently enabled the rapid acquisition of quantitative global heat-transfer measurements. The method, known as two-color relative-intensity phosphor thermography, is described in Refs. 5 and 29–31. Ceramic models, typically on the order of 12 in., can be fabricated rapidly, and a range of parameters, including AOA, sideslip, Reynolds number, Mach number, and control-surface deflection angle, can be investigated. For the X-34 heating studies,[32] results were obtained using this technique in the Langley 31-Inch Mach-10 and 20-Inch Mach-6 air facilities. These facilities are described in detail by Micol in Ref. 33. Digital optical measurements allow the rapid processing of data using Merski's IHEAT[5] code. In addition to the global images available, spanwise and chordwise cuts can be presented for comparison with engineering or detailed solutions. Reference 5 reports the uncertainty levels for the phosphor data obtained in the 20-Inch Mach 6 tunnel to be from 8 to 15%, depending on the surface temperature.

Flow visualization techniques are also used to complement the surface heating tests. The oil-flow technique is used to highlight surface streamline patterns. For the X-34 a stainless-steel model, painted black and coated with white pigmented oils, was tested in both the Mach-6 and the Mach-10 facilities. The Mach-6 facility, equipped with a schlieren system that shows the density variation in the flowfield, was used to highlight the existing shock patterns. These techniques, although qualitative in nature, represent an important contribution to the heat-transfer analyses by highlighting regions of the vehicle that may require detailed analysis.

TPS Considerations

OSC chose a TPS that utilizes thermal blankets over the acreage of the vehicle and ceramic tiles in the stagnation regions of the nose and the leading edges. This decision enabled OSC to take advantage of previously demonstrated TPS technologies and to incorporate advancements that have improved the operational characteristics of these systems.[3] A chief advantage of the flexible blankets is that

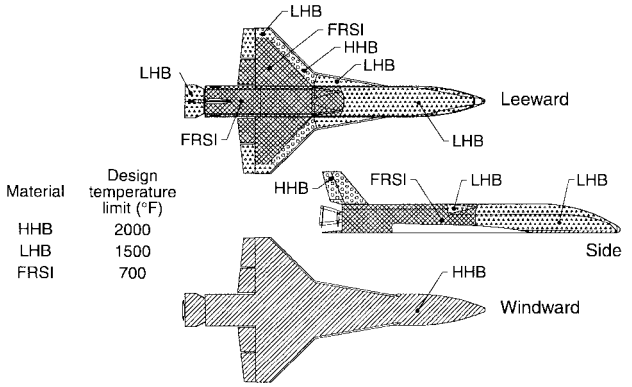

Fig. 3 X-34 TPS blanket layout.

they can be adhesively bonded to a nonsmooth surface. Also, the blankets' insulative characteristics lessen the impact to the structure because of uncertainties in external heating. However, the quilted-blanket design presents a fairly rough surface and is more likely to induce turbulent flow than would a smooth surface. Another issue that may impact vehicle operability, an important program objective, is the use of blankets in areas of high shear stress. This technology has not been demonstrated. The TPS layout is shown in Fig. 3. Three types of blankets are utilized on the X-34 vehicle, depending on the peak temperatures expected. The first, a low heat blanket (LHB), is used for regions expected to experience temperatures no greater than 1500°F. This blanket is similar to the flight-certified blanket currently in use on the leeward regions of the Shuttle Orbiter. The second type of blanket is the high heat blanket (HHB) designed for reuse at temperatures up to 2000°F. This blanket is used over the majority of the windward surface. In this blanket, the Astroquartz fabric and Q-felt insulation of the LHB are replaced with Nextel 440 and Saffil insulation, respectively, increasing its temperature capability. The LHB and the HHB are assumed to be coated with protective ceramic coating (PCC),[34] a high-emissivity coating designed to improve radiant characteristics at high temperatures. Nomex felt blankets, also known as flexible reusable surface insulation (FRSI), are to be used in the lowest temperature regions, up to 700°F (primarily the side fuselage and the upper surface). The FRSI is coated with a white silicone. SIRCA tiles are used in the high- temperature stagnation areas. Design and analysis for the tile regions were performed at ARC.[2,4] The LaRC effort concentrated on the blanket areas of the vehicle. Areas of concern immediately noted were roughness-induced turbulent heating, the design of the interface between the tile and blanket systems, potential areas of shock impingement and shock interactions, use of blankets in the high-shear regions of deflected control surfaces, the zone of transition of the fuselage cross section from circular to square, and the vortices emanating from the strake-fuselage juncture. The tile/blanket interface design and the blanket performance in high shear environments were outside the scope of the LaRC effort.

Overview of Aerothermal Approach for TPS Design

This paper details the aerothermal environments prediction process as it has been applied to the X-34 effort. In the year and a half since LaRC began this effort, the thermal environment predictions have evolved from preliminary heating estimates limited to the stagnation areas and the windward centerline, to an integrated analysis for 83 representative points on the vehicle, including off-centerline windward, leeward, and side fuselage locations. Prior to the acquisition of any wind-tunnel or computational data, an engineering heating method was employed. The obvious approach would have been to validate the engineering code results for the X-34 vehicle prior to implementation. However, this option was not possible because of the fast pace of the program. As wind-tunnel data became available,[32] comparisons were made with engineering predictions, and the engineering model was refined to reduce the conservatism in the predictions. An approach that coupled the experimentally measured heating distributions over the body with the time-dependent engineering predictions along the centerline was developed. This methodology was used to make the first predictions of the thermal environments over the acreage of the vehicle.

The program schedule and computational resources limited the number of detailed N–S heating solutions that could be used to benchmark the engineering methods. Instead, a coupled inviscid/boundary-layer method[19] was used. More solutions could be obtained along the trajectory because the inviscid/boundary-layer method requires fewer computational resources than an N–S method. Inviscid solutions were coupled with an approximate heating method[16] using the LATCH[15] code to provide heating distributions over the surface of the vehicle. The inviscid solutions were chosen to bound the heating-rate, AOA, freestream Mach-number, and Reynolds-number ranges over the flight profile, including the peak heating condition. Finally, the engineering code, MINIVER,[8] was used to interpolate the LATCH-generated spatial distributions in Mach number, AOA, and Reynolds number over the time of the trajectory. Thus, the time-dependent thermal environments necessary for TPS design were predicted through integration of wind-tunnel, detailed computational, and engineering methods. The thermal environments were then provided to the contractor for determining the acreage TPS requirements.

Preliminary Methodology

The first flight of the X-34 Technology Testbed Demonstrator was originally scheduled to occur prior to the end of 1998, approximately 2.5 years from the date of the award of the final contract. In this remarkably short time frame a vehicle system needed to be designed, materials ordered, components manufactured (including the engine that has yet to be demonstrated), ground facilities built, operational issues addressed, the vehicle assembled, the carrier aircraft modified, the vehicle mated, and the vehicle made ready to fly. The extraordinary pace of this program required that thermal environments be generated in parallel with design of the vehicle and development of the flight profile. The lead time required to set up for manufacture of the thermal blankets for the acreage and the tiles for the stagnation areas required preliminary definition of the TPS requirements very early on in the program. In light of these considerations, it was necessary to proceed with conservative engineering estimates of the heating environments before any wind-tunnel data or detailed computations were available and before a legitimate flight profile had been determined.

For the preliminary aerothermal predictions the windward centerline calculations were performed assuming sharp-cone entropy conditions. Flat-plate heating predictions were corrected for three-dimensional boundary-layer effects only through the use of the Mangler transformation. In the initial calculations no attempts were made to account for crossflow or regions of high localized heating due to flow phenomena such as shock interactions. The high probability of turbulent flow resulting from the inherent roughness of the quilted blanket system coupled with the low-altitude, high-Reynolds-number trajectory conditions led OSC to make the decision to base the TPS design on fully developed turbulent flow. Therefore, the heating calculations were based on turbulent levels.

The initial trajectory used in the calculations was denoted WAG18D and is presented in terms of Mach number, altitude, and AOA in Fig. 4. A more detailed discussion of the trajectory development and analysis is presented in a later section. Of all of

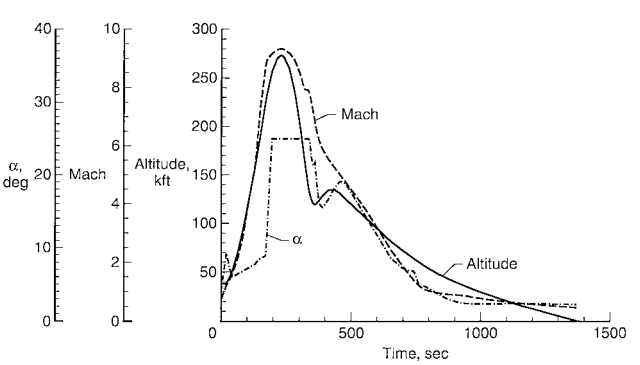

Fig. 4 WAG18D trajectory profile.

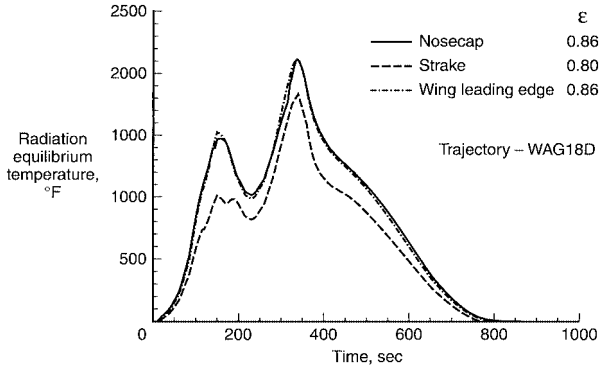

a) Stagnation area temperature–time histories

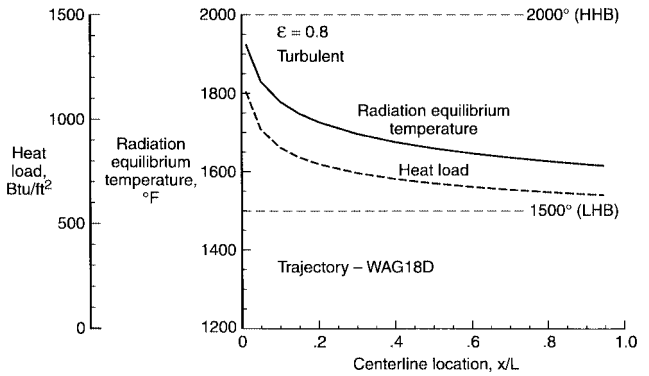

b) Windward centerline peak-heating distribution

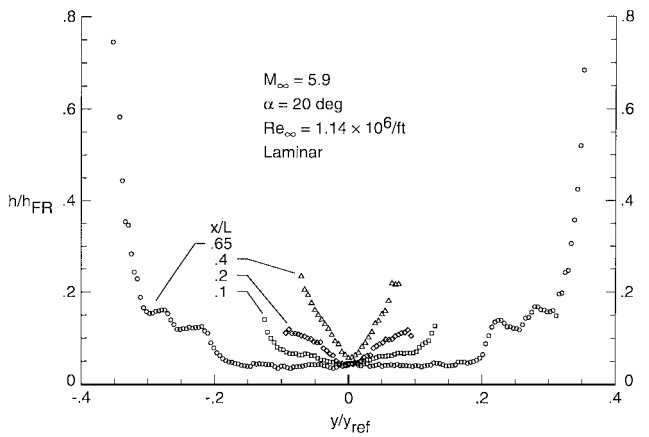

c) Experimental heating distributions

Fig. 5 Preliminary aerothermal predictions.

the trajectories examined, the WAG18D was found to be the most severe in terms of heating rates. A summary of the early engineering predictions is presented in Fig. 5. Figure 5a shows the calculated radiation equilibrium temperature time histories for the nosecap and the leading edges of the strake and wing. The radiative equilibrium temperatures are presented throughout this paper to provide a first-order assessment of the TPS selection. The calculations do not include heat conduction within the TPS and thus represent the maximum expected surface temperature levels. As noted previously, the nosecap and wing leading edge are constructed of SIRCA tile. An emissivity of 0.86 is therefore assumed for these areas. Comparison with similar calculations[35] performed by ARC show reasonable agreement. Figure 5b shows the peak radiation equilibrium temperature and the total-heat-load distribution values predicted for the windward centerline. A constant emissivity of 0.8 is assumed. The emissivity of the PCC coating used on the blankets varies from about 0.75 to 0.85 over this temperature range. Even for this severe trajectory case, the centerline heating environments should be well within the capability of the HHB. The environments provided to the blanket designers, Oceaneering Space Systems (OSS), were presented in terms of the heat transfer coefficient and recovery enthalpy time histories and initially included several points along the centerline.

Figure 5c illustrates typical spanwise heating distributions at several x/L stations on the windward surface. These data also were provided to OSS to aid in the initial blanket design. The laminar distributions, based on the 0.0153-scale model[32] of the X000912 (a pre-outer-mold-line-freeze configuration), were available for use in the initial blanket sizing to give some indication of the ratio of the heating at the vehicle chine relative to that at the centerline. Experience indicates that, although the local turbulent heating levels will be higher, the ratio of the chine to the centerline heating rates will be reduced in turbulent flow,[36] partially because of the reduced effect of crossflow on turbulent heating levels. The 20-deg AOA case was selected because it generally showed the highest heating amplification from the centerline to the chine. OSS was able to couple the predicted centerline heating time histories with the wind-tunnel heating data at several spanwise locations to make an initial determination of the blanket requirements over the windward surface. The initial blanket sizing and layout by OSS were based on these initial heating estimates and preliminary wind-tunnel heating distributions. Detailed computational solutions were not available until the outer mold line was frozen.

As additional wind-tunnel data became available, the data were used to confirm or modify the present engineering methodology. A sample of these data from Ref. 32 is presented in Fig. 6. Oil-flow

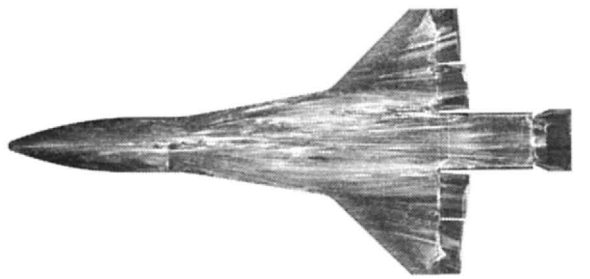

a) Oil-flow pattern (windside view, $\alpha = 15$ deg)

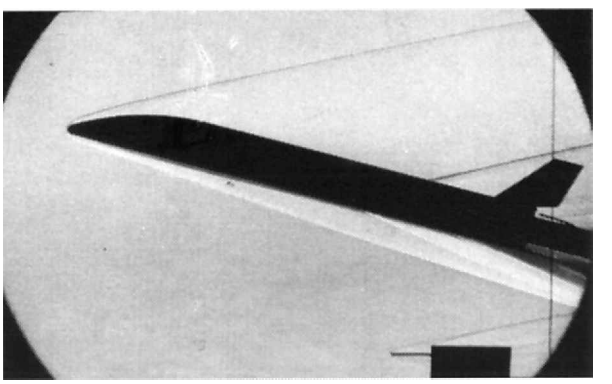

b) Schlieren image (side view, $\alpha = 15$ deg)

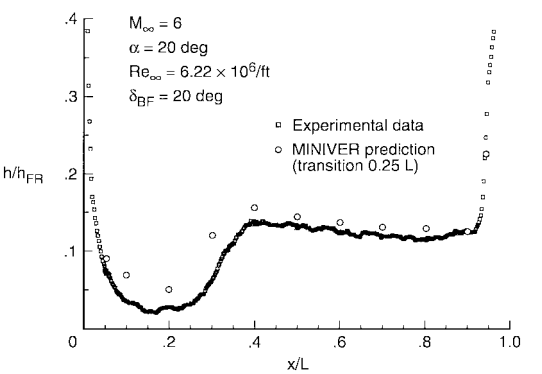

c) Comparison of MINIVER heat-transfer results with experimental data ($\alpha = 20$ deg)

Fig. 6 Preliminary wind-tunnel results.

views, similar to that presented in Fig. 6a, showed evidence of streamlines turning inward toward the model centerline (inflow) at AOA of 20 deg and lower. This result suggested that Baranowski's crossflow method[9] be modified to account for the thickening of the boundary layer along the centerline due to inflow. This modification has been shown to provide fairly good agreement with more detailed methods on vehicles such as the X-33 (Ref. 20). Schlieren views, such as that illustrated for a 15-deg AOA case in Fig. 6b, show a relatively strong conical shock, thus confirming the choice of sharp-cone entropy for the engineering analysis. Figure 6c shows a typical windward centerline experimental heating distribution normalized by a reference Fay–Riddell[37] stagnation point value. These data show clear evidence of transition at approximately $x/L = 0.25$. The results of the MINIVER heating predictions are shown to be in good agreement with the laminar and turbulent experimental data. The flight thermal environments were updated to reflect the modified methodology and recomputed. The change in maximum temperatures and total heat loads from the initial estimates were insignificant, and no modification of the blanket sizing was required. Although wind-tunnel tests often cannot match the actual flight Reynolds-number conditions or flow chemistry, comparisons such as that shown in Fig. 6c validate the analysis tools, which can then be applied to actual flight conditions.

Final Methodology

Trajectory Considerations

The rapid pace of the X-34 program required the environment predictions to be updated repeatedly as the vehicle configuration and trajectory were developed. All trajectories discussed herein were generated by OSC. The initial trajectory (WAG18D), available in July of 1996 and shown in Fig. 4, was based on a three-degree-of-freedom analysis (control deflection and trim requirements not considered) using the vehicle weight and performance available at that time. The maximum Mach number is about 9.3, and the maximum AOA is 25 deg. An updated trajectory profile, designated the DRM2, was made available at the Systems Requirements Review early in the fall of 1996. This trajectory, illustrated in Fig. 7a, reached a Mach number of only about 7.4 with the same maximum AOA (25 deg), indicating either reduced vehicle performance or a change in mission requirements. One feature noted in each of these early trajectories was the "bounce" that occurs at an altitude of about 110–120 kft. Once the outer mold line was frozen in December of 1996, higher-fidelity trajectories could be developed. As part of this effort, a guidance system had to be designed. OSC elected to eliminate the bounce in the trajectory in order to reduce the demands on the guidance system. The two trajectories shown in Figs. 7b and 7c are designated the X1004601 and the X1004701 trajectories, respectively. The altitude-time histories clearly show that the bounce has been successfully eliminated from both. Similar to the DRM2, the X1004601 has a peak Mach number of 7.4 and a maximum AOA of 25 deg. The X1004701, on the other hand, has a peak Mach number of 8.6 and a maximum AOA of 30 deg. It would be expected that the latter trajectory would yield the more severe windward heating environment with a possible reduction on the leeward side because of the increased AOA. However, at the request of OSC, LaRC provided all thermal environments based upon the X1004601 flight conditions. Possible reasons for OSC's initial selection of this trajectory to be used for blanket design are discussed in this section.

Figure 8 illustrates a comparison of the four trajectories in terms of reference heating levels. The reference levels are based on a Fay–Riddell calculation of the stagnation heating to a 1-ft sphere, corrected for a hot wall. These results indicate that the original trajectory (WAG18D) would probably subject the vehicle to the highest temperatures, requiring more extensive use of the high-temperature blankets, whereas the X1004701 would result in the greatest heat loads, possibly requiring greater TPS thickness. The peak heating levels for all of the newer trajectories are similar and significantly lower than those for the initial design trajectory.

Hot wall heating results presented in Fig. 9a show that the X1004701 trajectory presents somewhat more severe environments than the X1004601. A cold-wall heating comparison, presented in Fig. 9b for the same trajectories, suggests the opposite conclusion.

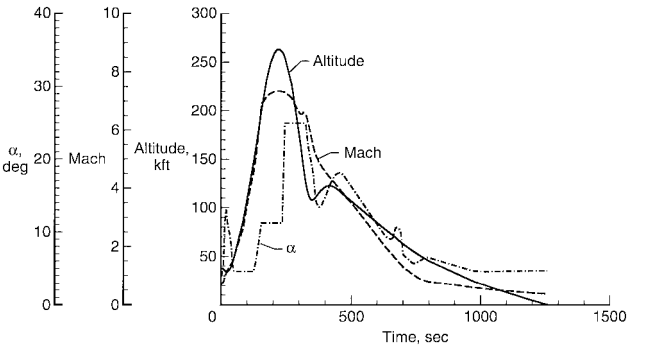

a) DRM2

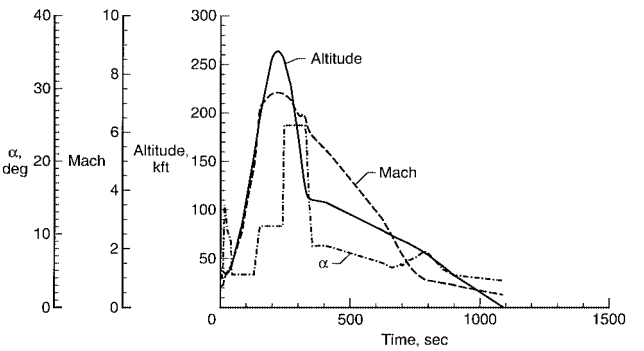

b) X1004601 (TPS blanket design trajectory)

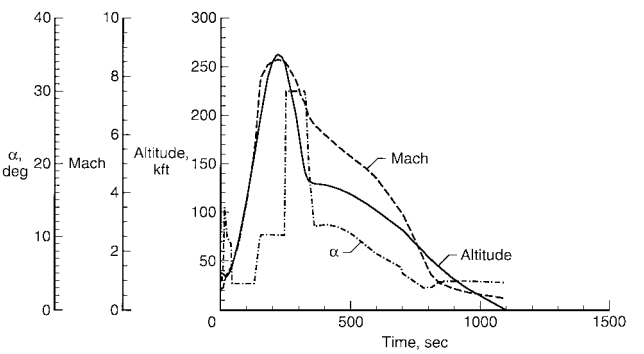

c) X1004701

Fig. 7 Trajectory profiles.

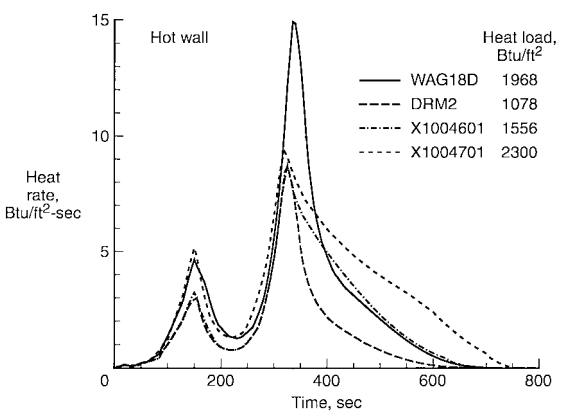

Fig. 8 Reference heating-rate comparisons for the design trajectories.

Trajectory codes such as POST[38] typically use a cold-wall heating indicator, and it is likely that these cold-wall results led to the OSC decision to base the blanket design on the X1004601 trajectory. Obviously, for flight conditions similar to those for the X-34 where the ratio of the wall enthalpy to recovery enthalpy is fairly high (approximately 0.4), the hot-wall heating rate would be a more appropriate parameter for use during trajectory development. This observation, together with the information required to assess the differences in the hot-wall heating levels for the

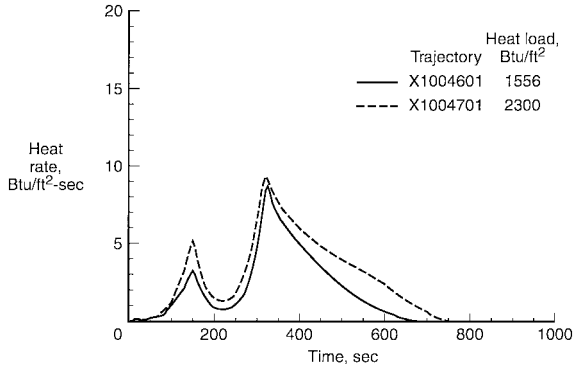

a) Hot-wall reference heating-rate time histories

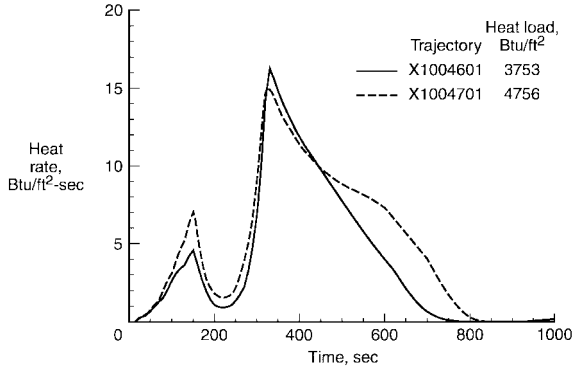

b) Cold-wall reference heating-rate time histories

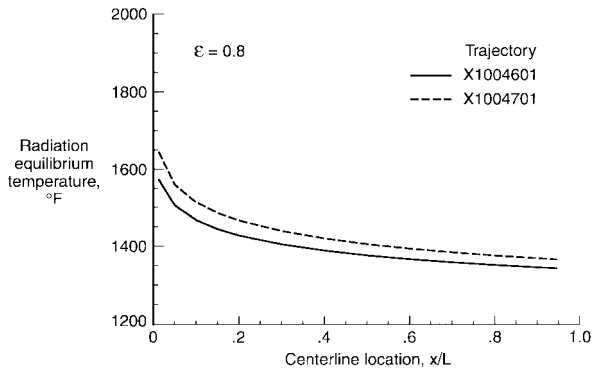

c) Windward-centerline peak-temperature distributions

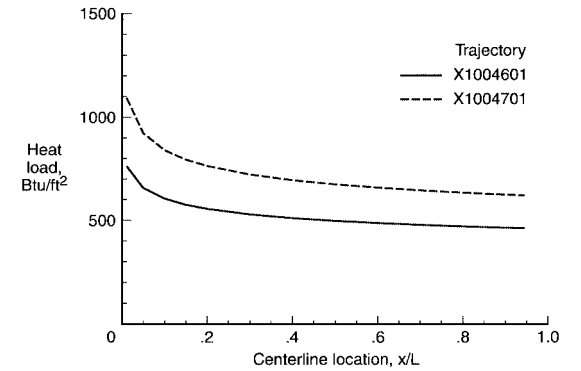

d) Windward-centerline peak-heat-load distributions

Fig. 9 Heating comparison of the X1004601 and the X1004701 trajectories.

X1004601 and the X1004701 trajectories, was provided to the contractor.

Figures 9c and 9d illustrate the peak temperature and heat-load distributions, respectively, along the windward centerline for the two TPS design trajectories used: X1004701 and X1004601. Similar to the results shown for the reference heating (hot-wall), the temperatures and the loads are generally greater for the X1004701 trajectory than for the X1004601.

Table 1 LATCH solutions

Time, s	Case #	AOA, deg	Mach number	Re_∞/ft	$\dot{q}_{ref}$ (hot), Btu/ft^2-s
145	7	9	6	1.9×10^4	3.0
152	4	11	6.83	1.4×10^4	3.1
330	1[a]	23	6.32	2.8×10^5	8.3
340	5[a]	15.22	6	3.6×10^5	7.3
355	3	8	5.8	3.8×10^5	6.5
578	6	6.48	3.6	7.5×10^5	0.9
334	8[b]	20.3	6.17	3.2×10^5	7.8

[a] Viscous solutions available.
[b] Additional LATCH solution obtained to check interpolation validity.

Table 2 Trajectory application of LATCH solutions for interpolation

Time, s	Case #	AOA, deg	Mach number	Re_∞/ft	$\dot{q}_{ref}$ range (hot), Btu/ft^2-s
0–137	6	4–14	0.7–5.2	3.0×10^4–1.5×10^6	0.1–2.5
145	7	9	6	1.9×10^4	3.0
150–240	4	10.5–11.1	6.7–7.3	1.1×10^3–1.5×10^4	0.9–3.2
242–331	1	23–25	6.3–7.3	1.1×10^3–2.8×10^5	0.9–8.3
340	5	15.22	6	3.6×10^5	7.3
355	3	8	5.8	3.8×10^5	6.5
578–714	6	6.6–5.5	1.6–3.5	7.7×10^5–8.5×10^5	0–0.9

Flow Condition Selection and Application

For trajectory and TPS trade studies an efficient approach may be to produce a large number of aeroheating solutions over a range of Mach number, Reynolds number, and AOA. For a specific trajectory, interpolation of the resultant heating database should be sufficient. The available time and resources precluded use of that approach here. The data set was limited to six solutions. The flight conditions were selected along the X1004601 trajectory at the request of OSC. Engineering judgment was required to choose the appropriate application of this solution set over the trajectory.

The trajectory points chosen (given by case numbers) and the associated parameters are listed in Table 1. Case 2, not shown, was not used to anchor the engineering results because the inviscid solution was based on a coarser grid than case 1, which was computed for the same trajectory condition. LATCH solutions were available at all conditions, whereas N–S solutions were available only for cases 1 and 5. Case 8, discussed later in the paper, was used as a check case to verify the interpolation scheme. Cases were selected to include the peak heating on ascent and descent and to represent variations in AOA and an appropriate range of Reynolds numbers. Figure 10 shows the time histories of altitude (Fig. 10a), Mach number (Fig. 10b), AOA (Fig. 10c), Reynolds number per foot (Fig. 10d), and reference heating rate (Fig. 10e). The trajectory times selected for the LATCH (inviscid/boundary layer) solutions are noted on each plot, as are the times at which the viscous solutions were generated. Because the majority of the high-heating portion of the trajectory has a small variation in Mach number and the flow state is defined to be turbulent, the primary influence on the heat-transfer distributions is the AOA. As shown in Fig. 10c, the AOA range is captured fairly well over the high heating portion of the entry (Fig. 10e). The point at 330 s (23 deg) should adequately represent the peak heating to the windward surface while that at 355 s (8 deg) should represent the highest heating on the leeward surface because of the low AOA. The case at 340 s (15 deg) provides heating distribution definition where the AOA is changing rapidly.

TPS sizing required computations to be performed at small time increments throughout the trajectory. A time step of 2 s was found to provide sufficient accuracy to define the changes in temperature experienced on the design trajectory. Referring to Fig. 10e, the majority of the heating will occur between 100 and 600 s making the case selection before and after those times less critical. Wherever a solution was available, it was applied. Table 2 lists the trajectory times at which the six solution cases were applied. Additionally, this table lists the corresponding range of AOA, Mach, and Reynolds numbers. In the time from 100 to 600 s, AOA was given priority in

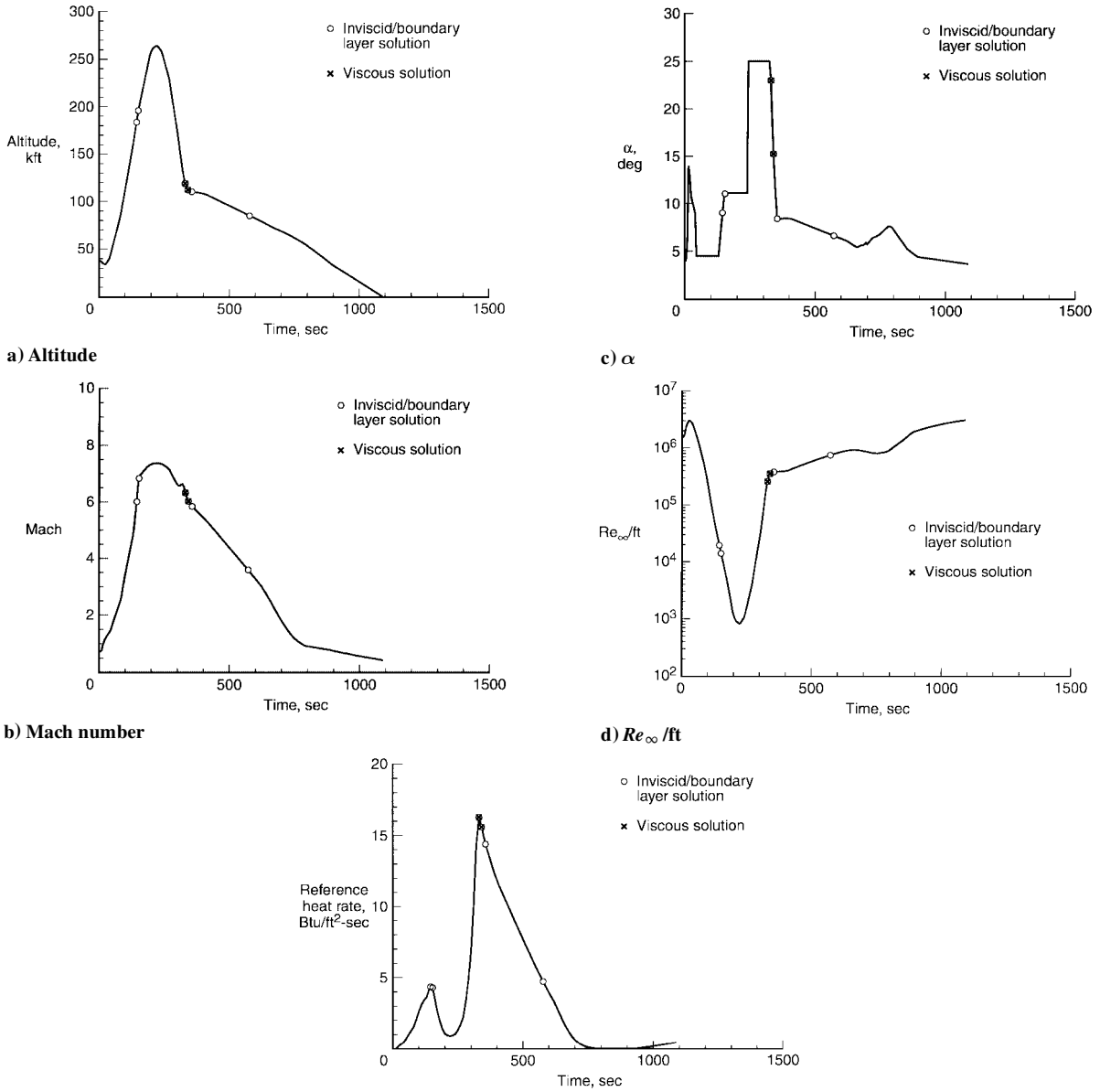

Fig. 10 X1004601 trajectory profile.

case selection. Comparison of the conditions in Table 2 with those in Table 1 for the design cases shows that Mach numbers generally did not vary significantly from the design point used. In some cases Reynolds number is seen to vary substantially from the design case. However, because a fully turbulent boundary layer was assumed for all heating distributions this variation was not considered critical. Where two times are listed, the distributions were held constant (but not the MINIVER reference). Times were generally chosen such that the flight AOA corresponded to those of the detailed solutions, thus allowing linear interpolation from one time step to the next.

Code Validation

Comparisons are presented in this section to demonstrate the validity of the more detailed techniques, as well as to further demonstrate the applicability of the MINIVER code. Several figures are used for the sake of clarity. Initially, the data are compared to the MINIVER predictions. Then the MINIVER results are compared to the LAURA and to the LATCH results, respectively. Finally, comparisons of the predicted results are made at a flight-test condition.

All engineering predictions shown here are made using the modified methodology as described in the Preliminary Methodology section. In Fig. 11 the MINIVER engineering predictions for the windward centerline of a 0.0183-scaled X-34 model at a wind-tunnel condition of Mach 6, an AOA of 15 deg, and unit Reynolds number of 7.9 million are compared to thermographic phosphor data[32] and analytical predictions.[19,25] In Fig. 11a the MINIVER predictions are compared with the thermographic phosphor data where transition is evident at an x/L of approximately 0.25. Both laminar and turbulent MINIVER solutions are shown. Once again the data are presented in the form of h/h_{FR}. Good agreement with the data is evident for both the laminar and turbulent results. MINIVER's overprediction of the laminar results in the forward portion of the body is expected and results primarily from the use of sharp-cone entropy conditions in this region where the streamlines are likely to have passed through a higher angle shock, characterized by higher entropy conditions. In Fig. 11b the MINIVER calculations are compared with the LAURA solutions. Once again good agreement is noted, particularly downstream where sharp-cone entropy is most appropriate. Finally, in Fig. 11c the MINIVER predictions are compared with those from the inviscid/boundary-layer solution of LATCH. Reasonable agreement is demonstrated once again, although it is apparent by comparison with Fig. 11a that the LATCH solutions tend to overpredict the data and the viscous solutions (Fig. 11b) at centerline stations downstream of approximately $x/L = 0.6$. The difference appears, however, to be less than 10% for the turbulent comparisons and suggests some conservatism in the LATCH-based predictions.

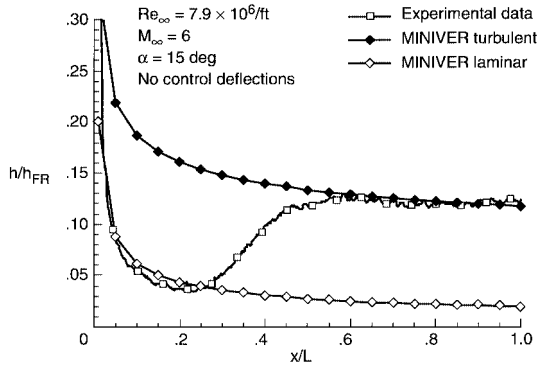

a) Experimental data (thermographic phosphor)

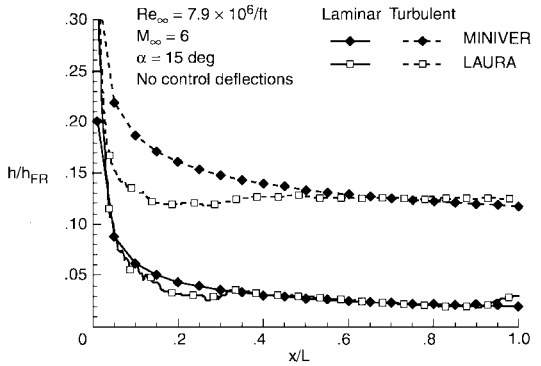

b) LAURA viscous results

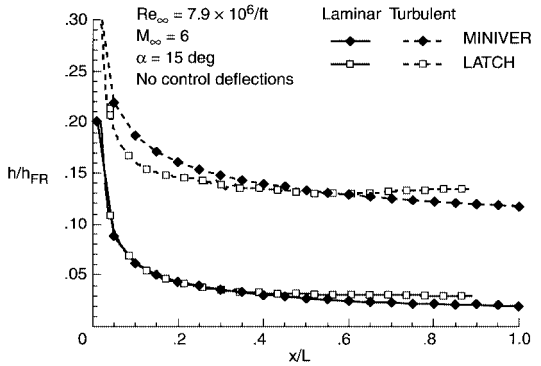

c) LATCH results

Fig. 11 MINIVER results compared at wind-tunnel test condition.

Figure 12 presents the MINIVER engineering prediction of turbulent heating rates along the windward centerline for the full-scale vehicle at the peak-heating flight condition ($t = 330$ s) on the X1004601 trajectory. Downstream of the 200-in. station, where the sharp-cone-entropy assumption is more appropriate, good agreement is shown with the LAURA and LATCH results.

A MINIVER-generated radiation equilibrium temperature-time history is shown in Fig. 13 for a representative location on the windward centerline for the X1004601 trajectory. The LATCH-generated values are shown for comparison. Even without adjustment, the MINIVER prediction of the temperatures is in excellent agreement with the LATCH predictions. Where any noticeable differences exist, MINIVER tends to overpredict and results in the conservative estimates desired. Particularly in regions of steep temperature gradients, the LATCH and MINIVER computed temperatures differ. The LATCH equilibrium wall temperatures were computed at a given trajectory time. For this study the time history solutions generated with the MINIVER code used the equilibrium wall temperature from the previous time step, previously noted to be small. Thus, this solution procedure results in slight differences in the temperature values. This case is typical of the MINIVER/LATCH agreement shown along the windward centerline for stations downstream of the nose region.

Comparisons of the MINIVER predictions with wind-tunnel data and detailed solutions at flight conditions suggest that the modified heating methodology yields heating rates that are somewhat conservative over the forward portion of the vehicle but predict the environments over the remainder of the acreage with reasonable accuracy. This conservatism, in combination with the more severe trajectory originally considered, suggests that the blanket TPS designed using the original environments provided and the WAG18D trajectory should be sufficient to handle both the maximum temperatures and total heat loads associated with the refined trajectories now available.

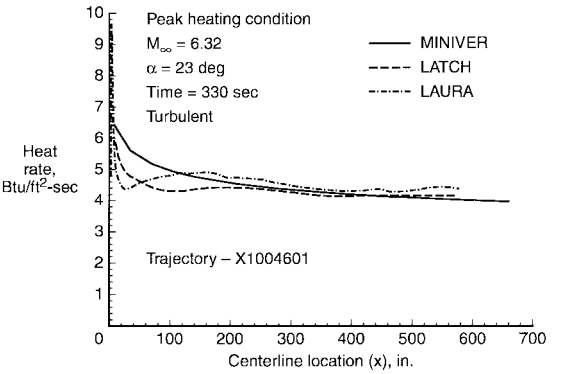

Fig. 12 MINIVER/LAURA/LATCH predictions compared at flight condition (case 1).

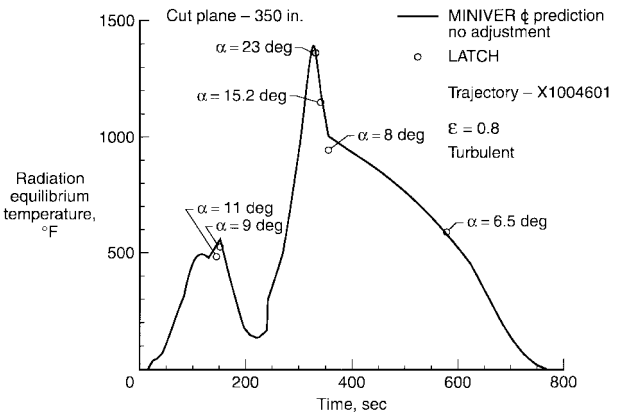

Fig. 13 MINIVER temperature comparison with LATCH results.

Coupled Procedure

The six LATCH solutions identified in Table 1 were used to anchor the engineering results. The engineering solutions were then used to interpolate in time to provide the required aerothermal environments at 83 body locations. The body locations examined were carefully selected to include regions of high heating, e.g., shock-shock interactions and imbedded vortices. The aerothermal environments were provided to the contractor in the form of time-dependent heat-transfer coefficients and recovery enthalpies (adiabatic wall enthalpies) like those shown in Fig. 14. These time-dependent environments were used to size the blankets, and the split-line locations for the different blanket materials (HHB, LHB, and FRSI) were determined using results from the detailed solutions.[19,25] The grid for the detailed solutions did not model TPS roughness, and thus potential increases in the turbulent heating were not determined in the detailed calculations. Therefore, the possible heating augmentation because of surface roughness was not included in the engineering results.

Centerline Adjustments

Figure 15 shows a typical comparison of MINIVER and LATCH heat-transfer coefficients for the windward centerline. This particular figure shows the heating comparison at 330 s on the X1004601 trajectory. Plots such as this were used to determine the factors necessary to correct the MINIVER prediction to match the LATCH value. The ratio of h_{cl} (the LATCH value) to h_{min} (the MINIVER prediction) was determined for 14 locations along the windward

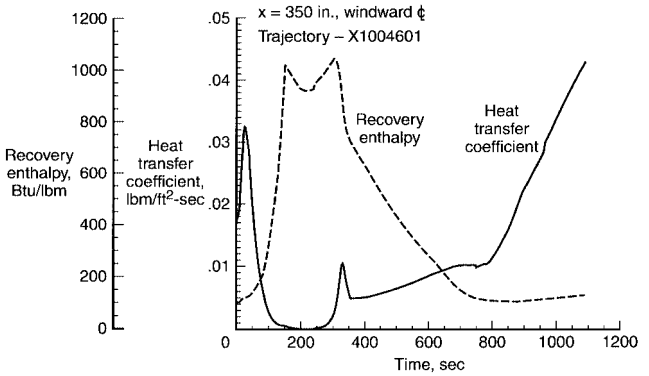

Fig. 14 Typical heat-transfer-coefficient and recovery-enthalpy time histories for blanket design.

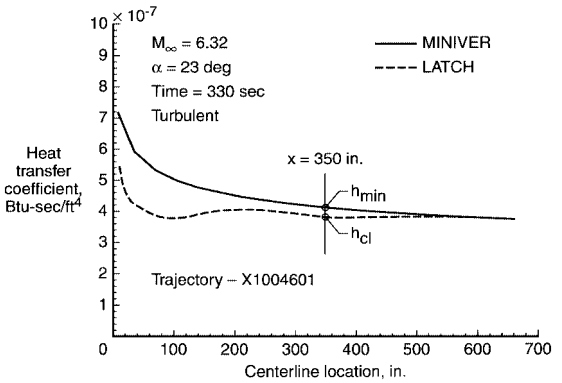

Fig. 15 MINIVER/LATCH windward-centerline heat-transfer coefficient comparison for peak heating case (case 1).

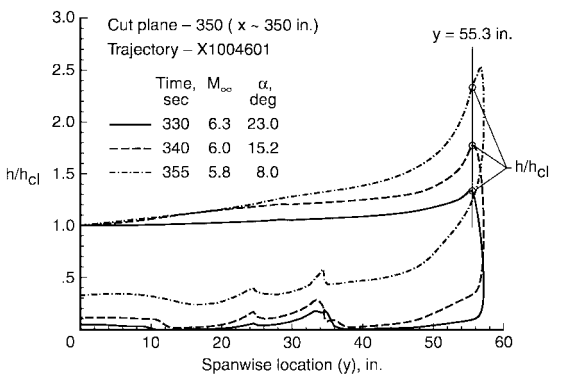

Fig. 16 Typical turbulent circumferential heating distributions from LATCH.

centerline from a point approximately 15 in. aft of the nosecap to approximately 560 in., which is the farthest aft location for which a LATCH solution was calculated. This procedure was repeated for each trajectory condition for which a LATCH solution was available, a total of six in this case.

Off-Centerline Adjustments

Once the adjustment factors were determined for the centerline, an additional correction had to be determined to adjust the predictions to match the heating distributions at locations away from the centerline. Figure 16 presents typical circumferential heating distributions for three different times along the X1004601 design trajectory representing AOA of 8.0, 15.2, and 23 deg. The data are presented as an h/h_{cl} distribution for a cut plane[19] located at an axial station of 350 in. The increasing influence of inflow with reduced AOA is evidenced by the corresponding increase in heating amplification at the most outboard locations. For each solution and each cut plane factors were evaluated at a sufficient number of spanwise locations to adequately define the distribution (typically three to five points) such that linear interpolation between points would yield reasonable agreement with the detailed solution. For each cut plane the location of maximum heating was selected as one of these locations. This selection ensured that the peak temperature would be captured for blanket TPS design. The h/h_{cl} factors and the centerline factors (h_{cl}/h_{min}) were used to determine the required MINIVER adjustment factor. The local heat transfer coefficient h was calculated using the following equation:

$$h = h_{min} \times (h_{cl}/h_{min}) \times (h/h_{cl}) \quad (1)$$

where h_{cl}/h_{min} is evaluated at the appropriate centerline location, h/h_{cl} is evaluated at the desired spanwise position along the cut plane, and h_{min} is calculated as a function of time using standard engineering techniques in MINIVER. Thus, a MINIVER-generated centerline heating-rate time history could be corrected to yield the time-dependent thermal environment for any point on the body for which the appropriate set of factors has been determined.

Results

In this section, several radiation-equilibrium time histories will be presented. As noted previously, the calculated temperatures are presented only to provide an assessment of the TPS selection. The calculations do not include heat conduction within the TPS, and thus represent the maximum expected surface temperature levels. The locations for the calculations include the windward and leeward surfaces as well as the side surface. As previously noted for the selection of the 83 body points, attention was given to selecting body points in regions of high localized heating.

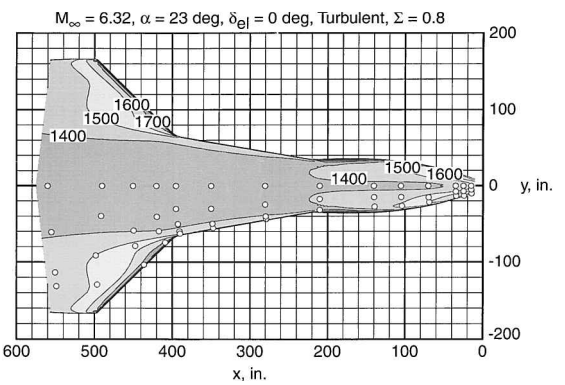

a) Windside view (case 1)

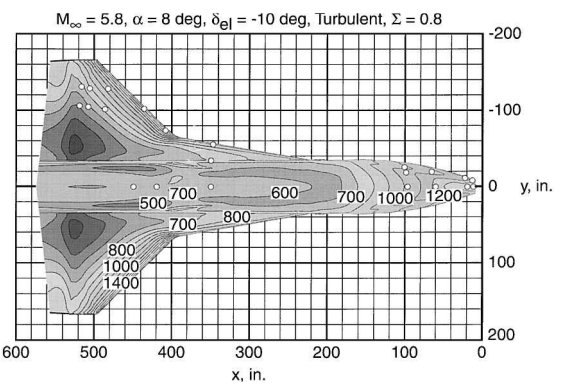

b) Leeside view (case 3)

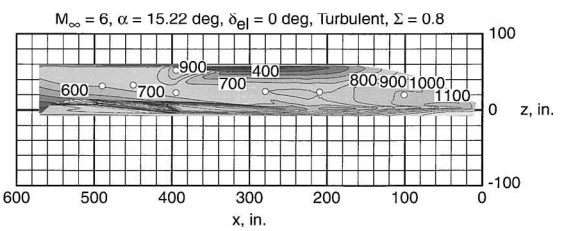

c) Side view (case 5)

Fig. 17 Body point locations for time-dependent environment calculations (LATCH temperature contours, °F).

Analysis Locations

Figure 17 shows the locations (standard body-oriented x, y, z coordinate system with the x-axis origin at the nose; the y axis oriented out the starboard wing; and z defined by the right-hand rule) selected for calculation of the time-dependent aerothermal environments. The locations are superimposed on windward, leeward, and side views of the X-34 vehicle. LATCH results[19] are indicated in terms of temperature contours. Fifty-two windside locations were chosen based on the peak-heating case, case 1 (Mach = 6.32, AOA = 23 deg, time = 330 s), and are shown in Fig. 17a. They include locations on 14 cut planes. Points along the cut planes were selected such that linear interpolation between the points would generally yield a fair representation of the results. Two additional points on the centerline of the undeflected body flap were calculated ($x = 630$ and 660 in.) but not shown because the LATCH solution did not extend to that region.

Comparison of all of the LATCH solutions confirmed that case 3 (Mach = 5.8, AOA = 8 deg, time = 355 s) represented the worst-case heating on the leeward surface, primarily because of the low AOA at relatively high-reference heating levels. Shown in Fig. 17b, superimposed on the LATCH results for case 3, are the locations of the 22 leeward points for which time histories were provided. These included eight points on the wing, two on the strake, and the remainder on the fuselage. No points were provided for the deflected elevons, apparent in Fig. 17b at roughly the 530-in. station.

Time-dependent environments at additional locations on the side of the fuselage also were provided. These locations are marked on Fig. 17c, which also shows the LATCH temperature contours for case 5 (Mach = 6, AOA = 15.22 deg, time = 340 s). An area of particular concern is the juncture where the rounded forward fuselage transitions to the square cross section, given by x and z locations of approximately 400 and 50 in., respectively. This area is protected by the LHB (see Fig. 3).

Windward Surface Heating

Windside time-dependent aerothermal environments have been calculated for a total of 52 points. Typical results, presented in the form of radiation-equilibrium time histories, are shown in Fig. 18. Figures 18a–18d represent calculations at four representative cut planes: $x = 15$, 70, 350, and 450 in. As can be seen in Fig. 17a, the two forward cut planes lie entirely on the fuselage, whereas the two aft cut planes include points on the strake and wing, respectively. The trends in the time histories are generally consistent: the outboard locations tracking the centerline results but with some amplification in heating. This amplification is particularly evident on the 450-in. cut plane near the leading edge of the wing (Fig. 18d). Assuming the radiation-equilibrium temperatures provide a conservative estimate of the surface temperature, the multiuse temperature limit of the HHB selected for use over this region (Fig. 3) is not exceeded for any of the points calculated.

Leeward Surface Heating

Time-dependent aerothermal environments have been calculated for a total of 22 points on the leeside of the vehicle. Figure 19 illustrates typical time-dependent results for this surface at four cut planes: $x = 15$, 70, 350, and 450 in. Once again, the two forward cut planes lie entirely on the fuselage, whereas the two aft cut planes include points on the strake and wing, respectively. As expected, maximum temperatures are shown to be significantly lower on the lee surface than those seen previously on the windward surface (Fig. 18). The occurrence of peak heating on the leeward surfaces is delayed slightly from that on the windward surface. Unlike the windward surface, heating on the leeside lags the peak reference heating slightly and occurs as the AOA drops rapidly. The character of the heating on the leeward surface also differs from that on the windward surface in that the heating, although not as high in magnitude, does not drop off as rapidly after peak heating. As can be seen by comparing the blanket layout in Fig. 3 to the analysis locations shown in Fig. 17b, all of these locations [with the exception of the point on the 450-in. cut plane near the leading edge of the wing (SIRCA) and the centerline locations on the 350- and the 450-in. cut planes (FRSI)] are protected with the LHB, which has a maximum-use temperature of 1500°F. Upon the examination of the time histories in Fig. 19, this temperature appears unlikely to

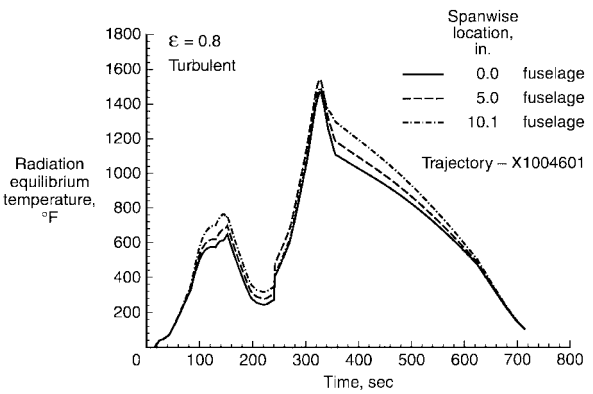

a) Cut plane: 15 in.

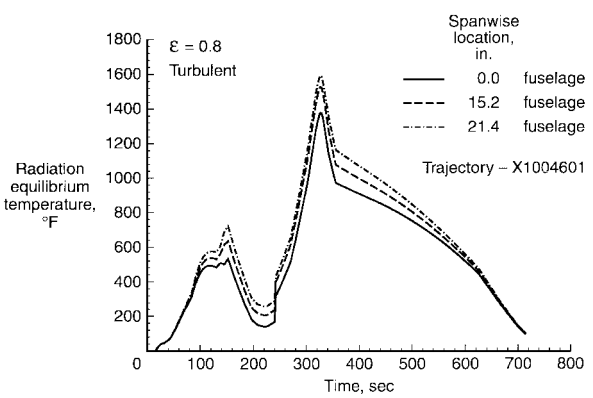

b) Cut plane: 70 in.

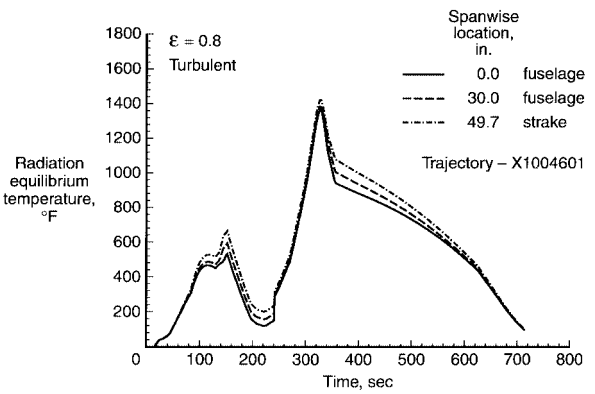

c) Cut plane: 350 in.

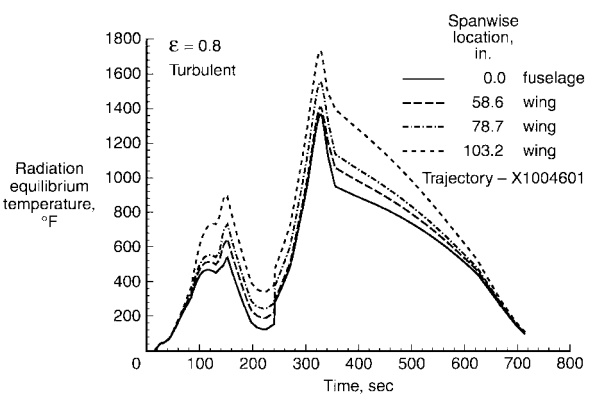

d) Cut plane: 450 in.

Fig. 18 Typical windside temperature–time histories.

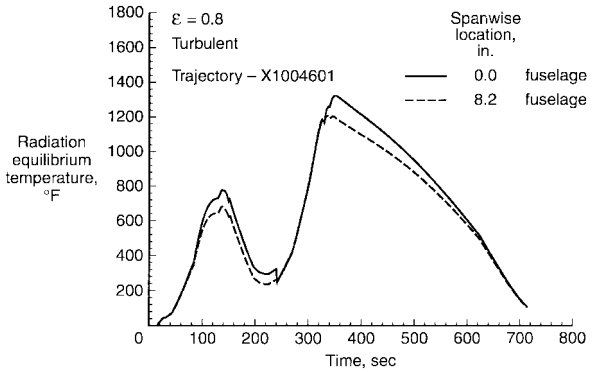

a) Cut plane: 15 in.

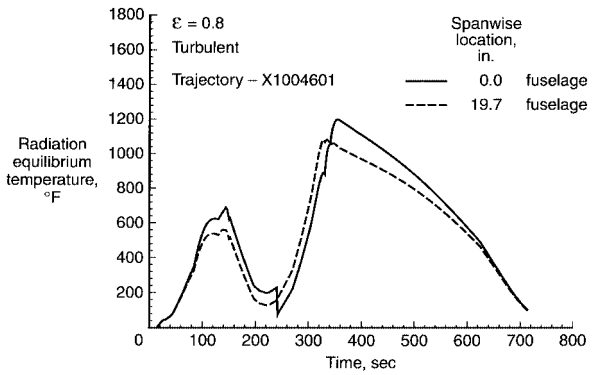

b) Cut plane: 70 in.

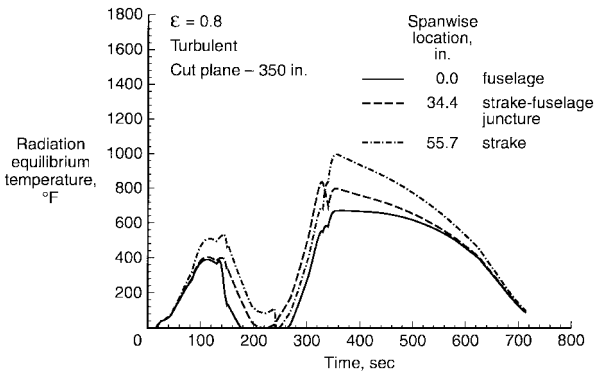

c) Cut plane: 350 in.

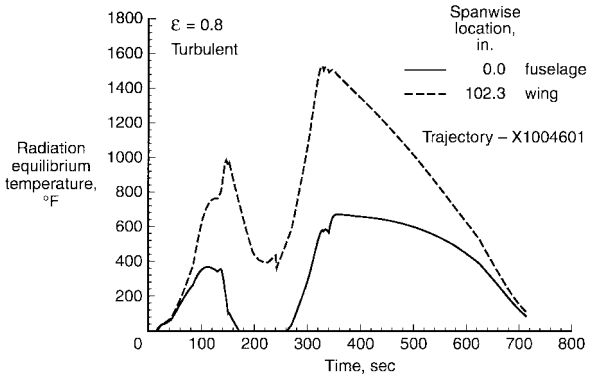

d) Cut plane: 450 in.

Fig. 19 Typical leeside temperature–time histories.

be exceeded at any of these locations. Even the point near the leading edge of the wing on the 450-in. cut plane exceeds 1500°F only slightly (Fig. 19d). The SIRCA tile at the leading edge should be sufficient to accommodate this thermal environment.

The majority of the lee surface of the wing is to be protected by FRSI as is the aft portion of the leeward fuselage. Figure 20 illustrates the radiation-equilibrium time histories for two locations on the leeward surface of the wing. Both points appear to exceed

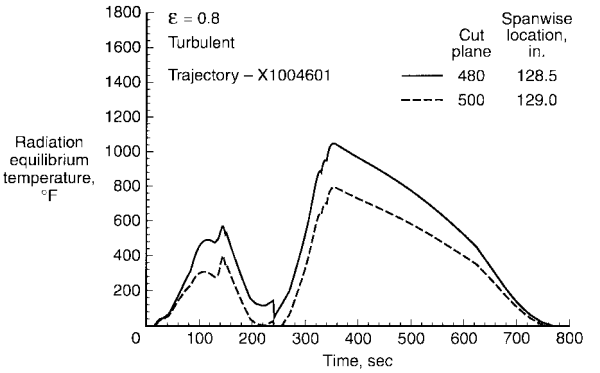

Fig. 20 Typical leeward-wing temperature–time histories.

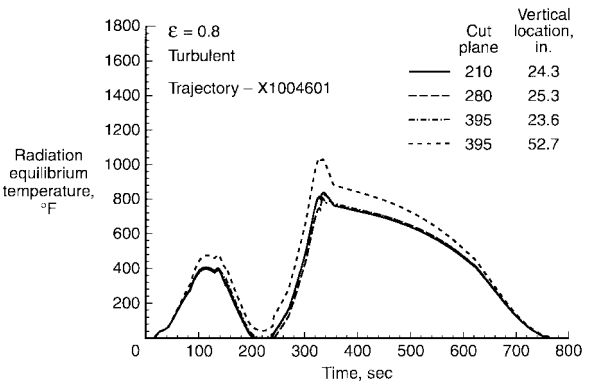

Fig. 21 Typical side-surface temperature–time histories.

the FRSI capability of 700°F. However, at the time of this study the TPS had not been laid out in sufficient detail to determine whether the locations (shown in Fig. 17b) in question would be protected by FRSI or LHB. The information provided enabled OSC to adjust the split lines if necessary. The centerline locations on the 350- and the 450-in. cut plane (mentioned previously) do appear to lie within the region protected by FRSI. The predictions shown in Figs. 19c and 19d, respectively, for these points show maximum temperatures just within the FRSI capability.

Side-Surface Heating

Time-dependent aerothermal environments also have been calculated for seven side-surface locations, including a point at the 395-in. cut plane where the body cross section transitions from circular to rectangular. Figure 21 illustrates some typical results for the side fuselage. Except for the fuselage transition zone, the peak temperatures along the fuselage aft of 300 in. are in the 750–850°F range. With this result and the blanket distribution shown in Fig. 3, the fuselage regions that are protected by FRSI are likely to exceed the blanket temperature capability. The LHB used at the transition zone would be sufficient to withstand the maximum temperatures (approximately 1030°F) shown in Fig. 21.

Interpolated Result Verification

An additional LATCH inviscid/boundary-layer solution was calculated to test the validity of the interpolation scheme used to establish the time-dependent aerothermal environments shown here. The test case, identified as case 8 in Table 1, was computed for the flight condition at 334 s on the X1004601 trajectory. An inviscid solution at a Mach number of 6.17 and an AOA of 20.3 deg was used as input to the LATCH code to establish turbulent heating levels over the vehicle. Figure 22 shows some representative heating time histories as predicted using the techniques described in this paper. The predictions are shown for three points along the 350-in. cut plane, including the windward and leeward centerline and a point near the leading edge of the strake. The predicted heating rates and radiation-equilibrium temperatures are shown in Figs. 22a and 22b, respectively. The results of the new LATCH solution at 334 s are also shown. Differences in heating rates of less than 10%

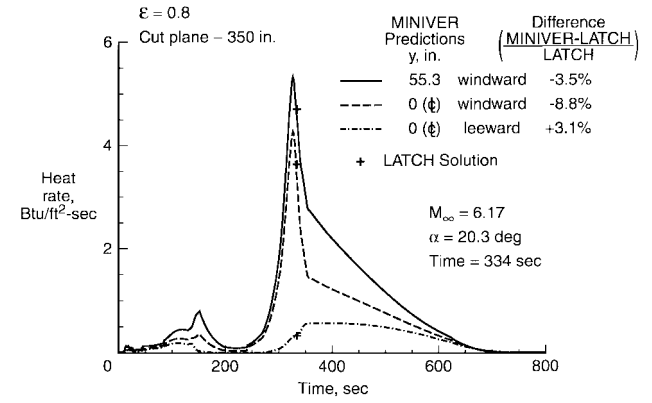

a) Heating rates

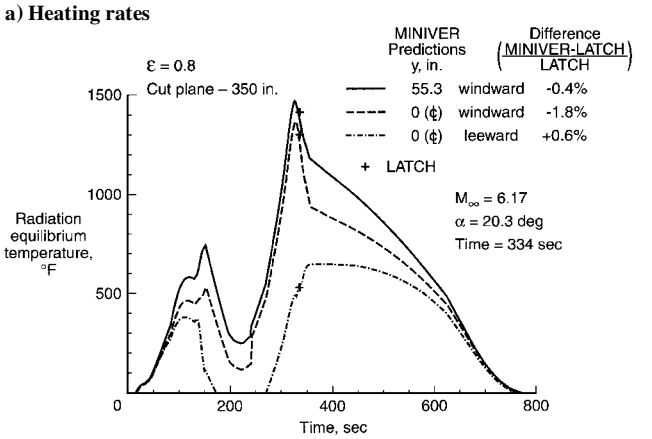

b) Temperatures

Fig. 22 Verification of MINIVER interpolation process.

are noted. The corresponding differences in temperature are significantly lower, less than 2%. Heat-transfer-coefficient discrepancies (not shown) were noted to be less than 3%. Similar results were observed for all other points examined. As noted previously, part of the disagreement is introduced simply because the radiation equilibrium temperature computed along a trajectory will not be equivalent to one computed at a constant freestream condition. The interpolated results are shown to compare well with the LATCH solution generated at the additional flight condition, demonstrating the validity of the approach used in this study. Thus, the techniques employed here enable prediction of time-dependent aerothermal environments with a sufficient degree of accuracy for TPS design.

Concluding Remarks

This paper has described the methodology by which the aerothermal environments for the X-34 have been predicted in sufficient detail to allow design of the TPS such that the survivability, as well as the reusability, of the flight vehicle is ensured to a high degree of certainty. Initial estimates of the aerothermal environments, provided before any wind-tunnel or detailed computational data were available, are shown to be conservative. Engineering results, validated against both experimental data and viscous N–S solutions, demonstrate good agreement. A combination of engineering methods, coupled with inviscid CFD solutions, is used to generate the detailed time-dependent environments over the surface of the vehicle. The interpolated engineering values are shown to be in good agreement with the more detailed results. However, the selection of the cases for detailed solutions is critical to the success of the interpolation. In particular, the AOA and Mach-number conditions must be matched adequately, and the conditions of peak windward and leeward surface heating must be captured. Selection of the peak heating conditions based on a cold-wall value has been demonstrated to be inappropriate for vehicles such as the X-34 that operate in flight regimes where the recovery-to-wall-enthalpy ratio is significant.

The aerothermal results presented in this paper have been used to design and size the blanket TPS on the X-34. The method described was formulated to take optimal advantage of the strengths of the engineering and experimental techniques together with those of the detailed flowfield codes. Minimal computational resources and time were required to provide sufficiently accurate, time-dependent aerothermal environments to design the X-34 blanket TPS. This method easily could be automated and applied to many of the fast-paced programs that are typical in today's design environment. In doing so, the conservatism inherent to any TPS designed using engineering methods alone could be reduced, potentially decreasing the vehicle weight and improving the payload capability.

References

[1]Freeman, D. C., Jr., Talay, T. A., and Austin, R. E., "Reusable Launch Vehicle Technology Program," IAF Paper 96-V.4.01, Oct. 1996.

[2]Milos, F. S., and Squire, T. H., "Thermostructural Analysis of X-34 Wing Leading-Edge Tile Thermal Protection System," *Journal of Spacecraft and Rockets*, Vol. 36, No. 2, 1999, pp. 189–198.

[3]Rasky, D. J., "Thermal Protection Systems for Future Reusable Launch Vehicles," SAE Paper 951618, July 1995.

[4]Palmer, G., and Polsky, S., "Heating Analysis of the Nosecap and Leading Edges of the X-34 Vehicle," *Journal of Spacecraft and Rockets*, Vol. 36, No. 2, 1999, pp. 199–205.

[5]Merski, N. R., "Global Aeroheating Wind-Tunnel Measurements Using Improved Two-Color Phosphor Thermography Method," *Journal of Spacecraft and Rockets*, Vol. 36, No. 2, 1999, pp. 160–170.

[6]"X-34," NASA NRA 8-14, March 1996.

[7]"Reusable Launch Vehicle (RLV), Small Reusable Booster, X-34," CAN 8-2, Jan. 1995.

[8]Engel, C. D., and Praharaj, S. C., "MINIVER Upgrade for the AVID System, Vol. I: LANMIN User's Manual," NASA CR-172212, Aug. 1983.

[9]Baranowski, L. C., "Influence of Cross-Flow on Windward Centerline Heating," McDonnell Douglas Astronautics Co., Rept. MDC E0535, St. Louis, MO, Dec. 1971.

[10]Schlichting, H., *Boundary Layer Theory*, 6th ed., McGraw-Hill, New York, 1968, pp. 235–237.

[11]Wurster, K. E., Zoby, E. V., and Thompson, R. A., "Flowfield and Vehicle Parameter Influence on Results of Engineering Aerothermal Methods," *Journal of Spacecraft and Rockets*, Vol. 28, No. 1, 1991, pp. 16–22.

[12]Wurster, K. E., and Stone, H. W., "Aerodynamic Heating Environment Definition/Thermal Protection System Selection for the HL-20," *Journal of Spacecraft and Rockets*, Vol. 30, No. 5, 1993, pp. 549–557.

[13]Baumgartner, R. I., and Elvin, J. D., "Lifting Body—An Innovative RLV Concept," AIAA Paper 95-3531, Sept. 1995.

[14]"Access to Space Study—Summary Report, Office of Space Systems Development," Office of Space and Systems Development, NASA, Jan. 1995.

[15]Hamilton, H. H., II, Greene, F. A., and DeJarnette, F. R., "Approximate Method for Calculating Heating Rates on Three-Dimensional Vehicles," *Journal of Spacecraft and Rockets*, Vol. 31, No. 3, 1994, pp. 345–354.

[16]Zoby, E. V., and Simmonds, A. L., "Engineering Flowfield Method with Angle-of Attack Applications," *Journal of Spacecraft and Rockets*, Vol. 22, No. 4, 1985, pp. 398–405.

[17]Zoby, E. V., "Approximate Heating Analysis for the Windward Symmetry Plane of Shuttle-Like Bodies at Large Angle of Attack," *Thermophysics of Atmospheric Entry*, edited by T. E. Horton, Vol. 82, Progress in Astronautics and Aeronautics, AIAA, New York, 1982, pp. 229–247.

[18]Hamilton, H. H., DeJarnette, F. R., and Weilmuenster, K. J., "Application of Axisymmetric Analog for Calculating Heating in Three-Dimensional Flows," *Journal of Spacecraft and Rockets*, Vol. 24, No. 4, 1987, pp. 296–302.

[19]Riley, C. J., Kleb, W. L., and Alter, S. J., "Aeroheating Predictions for X-34 Using an Inviscid Boundary-Layer Method," *Journal of Spacecraft and Rockets*, Vol. 36, No. 2, 1999, pp. 206–215.

[20]Hamilton, H. H., II, Weilmuenster, K. J., and Horvath, T. J., "Computational/Experimental Aeroheating Predictions for X-33 Phase II Vehicle," AIAA Paper 98-0869, Jan. 1998.

[21]Candler, G. V., Wright, M. J., and McDonald, J. D., "Data-Parallel Lower-Upper Relaxation Method for Reacting Flows," *AIAA Journal*, Vol. 32, No. 12, 1994, pp. 2380–2386.

[22]Wright, M. J., Candler, G. V., and Prampolini, M., "Data-Parallel Lower-Upper Relaxation Method for the Navier–Stokes Equations," *AIAA Journal*, Vol. 34, No. 7, 1996, pp. 1371–1377.

[23]Gnoffo, P. A., "Upwind-Biased, Point-Implicit Relaxation Strategies for Viscous, Hypersonic Flows," AIAA Paper 89-1972, Jan. 1989.

[24]Gnoffo, P. A., "An Upwind-Biased, Point-Implicit Relaxation Algorithm for Viscous, Compressible Perfect-Gas Flows," NASA TP-2953, Feb. 1990.

[25]Kleb, W. L., Wood, W. A., Gnoffo, P. A., and Alter, S. J., "Computational Aeroheating Predictions for X-34," *Journal of Spacecraft and Rockets*, Vol. 36, No. 2, 1999, pp. 179–188.

[26]Gnoffo, P. A., Weilmuenster, K. J., and Alter, S. J., "Multi-Block Analysis for Shuttle Orbiter Re-Entry Heating from Mach 24 to Mach 12," *Journal of Spacecraft and Rockets*, Vol. 31, No. 3, 1994, pp. 367–377.

[27]Weilmuenster, K. J., and Greene, F. A., "HL-20 Computational Fluid Dynamics Analysis," *Journal of Spacecraft and Rockets*, Vol. 30, No. 5, 1993, pp. 558–566.

[28]Wood, W. A., Riley, C. J., and Cheatwood, F. M., "Reentry-F Flowfield Solutions at 80,000 ft," NASA TM-112856, May 1997.

[29]Buck, G. M., "Automated Thermal Mapping Techniques Using Chromatic Image Analysis," NASA TM-101554, April 1989.

[30]Buck, G. M., "Surface Temperature/Heat Transfer Measurement Using a Quantitative Phosphor Thermography System," AIAA Paper 91-0064, Jan. 1991.

[31]Merski, N. R., "A Relative-Intensity Two-Color Phosphor Thermography System," NASA TM-104123, Sept. 1991.

[32]Berry, S. A., Horvath, T. J., DiFulvio, M., Glass, C., and Merski, N. R., "X-34 Experimental Aeroheating at Mach 6 and 10," *Journal of Spacecraft and Rockets*, Vol. 36, No. 2, 1999, pp. 171–178.

[33]Micol, J. R., "Hypersonic Aerodynamic/Aerothermodynamic Testing Capabilities at Langley Research Center: Aerothermodynamic Facilities Complex," AIAA Paper 95-2107, June 1995.

[34]Mui, D., and Clancy, H. M., "Development of a Protective Ceramic Coating for Shuttle Orbiter Advanced Flexible Reusable Surface Insulation (AFRSI)," *Ceramic Engineering and Science Proceedings*, Vol. 6, No. 7–8, 1985, pp. 793–805.

[35]Rivell, T., "Preliminary Design of the Thermal Protection System for the X-34 Reusable Launch Vehicle: SIRCA-15F Tiles," ARC X-34 Rept., approved by Timothy P. Castellano, NASA Ames X-34 Project Manager, Feb. 1997.

[36]Adams, J. C., Jr., "Implicit Finite-Difference Analysis of Compressible Laminar, Transitional, and Turbulent Boundary Layers Along the Windward Streamline on a Sharp Cone at Incidence," Arnold Engineering Development Center, AEDC-TR-71-235, Tullahoma, TN, Dec. 1971.

[37]Fay, J. A., and Riddell, F. R., "Theory of Stagnation-Point Heat Transfer in Dissociated Air," *Journal of Aeronautical Sciences*, Vol. 25, No. 2, 1958, pp. 73–85, 121.

[38]Brauer, G. L., Cornick, D. E., and Stevenson, T., "Capabilities and Applications of the Program to Optimize Simulated Trajectories (POST)," NASA CR-2770, Feb. 1977.

T. C. Lin
Associate Editor